# Final Report on DE-SC0001853

# Manipulating Light with Transition Metal Clusters, Organic Dyes, and Metal Organic Frameworks

**Principal Investigator**: Serdar Öğüt, University of Illinois at Chicago

**Grant Period**: December 1, 2012 through May 31, 2017

**DOE/Office of Science Technical Program Manager**: Dr. Mark Pederson

**Personnel Involved in the Project:** Dr. Linda Hung (postdoc), Bin Shi (student)

## Program Scope

The primary goals of our research program were to develop and apply state-of-the-art first-principles methods to predict electronic and optical properties of three systems of significant scientific and technological interest: transition metal clusters, organic dyes, and metal-organic frameworks. These systems offer great opportunities to manipulate light for a wide ranging list of energy-related scientific problems and applications. During this grant period, we focused our investigations on the development, implementation, and benchmarking of many-body Green's function methods ($GW$ approximation and the Bethe-Salpeter equation) to examine excited-state properties of transition metal/transition-metal-oxide clusters and organic molecules that comprise the building blocks of dyes and metal-organic frameworks.

# 1 Accomplishments and Results

## 1.1 Electronic and Optical Excitations in $TiO_2$ Nanocrystals

Motivated by the growing need for an accurate understanding of nanostructured $TiO_2$ driven by its various uses related to solar energy, we investigated the size and shape dependence of rutile $TiO_2$ nanocrystals (NCs) and studied trends in their electronic and optical properties using the *GW* approximation and TDDFT [1]. Ionization potentials (IPs) and electron affinities (EAs) were obtained via the perturbative *GW* approximation with an LDA starting point ($G_0W_0$@LDA) and the ΔSCF method (total-energy differences within DFT) for NCs up to 24 and 64 $TiO_2$ formula units, respectively.

Our work also allowed us to address some of the important technical considerations in applying the *GW* method to these relatively large (*e.g.* the $(TiO_2)_{24}$ NC has 644 valence electrons) and computationally challenging transition-metal-oxide nanostructures. In particular, we showed how to exploit quantum confinement to reduce the number of empty states in *GW* summations within a real-space framework. Since we use zero boundary conditions, in which the Kohn-Sham (KS) wavefunctions are required to vanish outside a spherical domain of radius $R$, for the confined systems we study, the KS eigenvalues of unoccupied states at high energies are significantly affected by the choice of $R$. Due to quantum confinement, the spectral width of a fixed number of unoccupied states as a function of $R$ scales as $R^{-2}$. If we fixed $N$ (the index of the highest DFT state included in the *GW* summations) and changed $R$, the *GW* summations would extend to different maximum energies (decreasing as $R$ increases), resulting in physically different Green's functions and polarizabilities due to the varying energy contributions. Instead, we showed that the appropriate comparison of *GW* calculations at different $R$ is not given by calculations with the same $N$, but by calculations that include summations over all empty states up to the state with some predetermined DFT eigenvalue $\varepsilon_N$. Fig. 1 shows the convergence properties for the EA of the smallest NC computed within the $G_0W_0$ approximation. As a function of $\varepsilon_N$, the computed EAs for $R = 12, 16$, and 20 a.u. all give the same *GW* energies, demonstrating that *GW* calculations are converged relative to simulation cell size. The results shown for $R = 10$ a.u., on the other hand, are significantly different from the rest of the computed EA values and converge to a different value, stemming from the fact that the DFT eigenvalue of the LUMO of this NC is not well converged at $R = 10$ a.u. as a function of $R$. Similar convergence properties are observed for the IP, and in general, our tests show that as long as $R$ is chosen sufficiently large so that the KS eigenvalues of the relevant states (*e.g.* HOMO and LUMO, for the computations of IP and EA, respectively) are converged, the size of the simulation cell does not affect the computed quasiparticle energies.

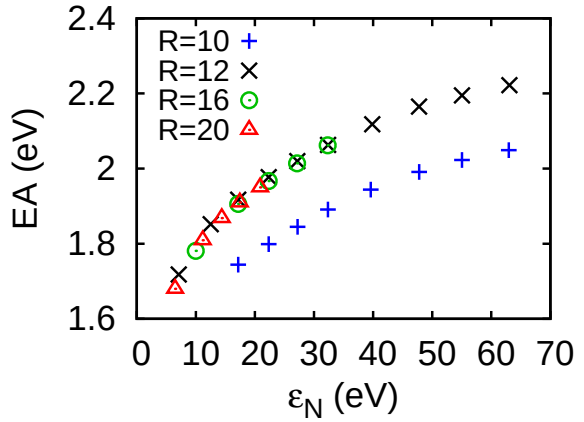


Figure 1: The EA of the $(TiO_2)_2$ NC at various levels of convergence in *GW*, for simulations performed in real-space spheres with radii ranging from $R = 10$ to 20 a.u. The $G_0W_0$ EA is plotted relative to the KS-DFT energy of highest unoccupied state included in each calculation, $\varepsilon_N$. Results are already converged with respect to radii at $R = 12$ a.u., but not at $R = 10$ a.u., for which the predicted EA value is ∼0.2 eV lower than the true EA value after achieving convergence with respect to $\varepsilon_N$.

This independence of IP and EA values with respect to the choice of $R$ can be exploited, so that one can choose the *smallest* possible simulation cell for which HOMO and LUMO are converged *at the DFT level*. Typically, convergence to within 0.1 eV in *GW* quasiparticle energies requires a convergence of ∼ 5 meV for the relevant DFT eigenvalue as a function of $R$. There are two important benefits of using a small $R$: First, the number of grid points, $N_{\text{grid}}$, in the physical domain is decreased ($N_{\text{grid}} \propto R^3$), which means that all the relevant Coulomb integrals can be evaluated more quickly. Second, and more importantly, the

confining smaller sphere means that fewer unoccupied states are needed to reach a given summation cutoff energy due to the quantum confinement of the simulation cell (also scaling approximately as $R^3$). For the $(TiO_2)_2$ NC, for example, a $GW$ calculation with $\varepsilon_N = 20$ eV for $R = 20, 16$, and 12 a.u. requires 943, 516, and 239 states, respectively, which underscores the tremendous computational savings that quantum confinement enables in $GW$ computations of confined nanostructures.

Fig. 2(a) shows the IPs and EAs computed using the total-energy differences ($\Delta$SCF method) and the $G_0W_0$ method as a function of the number of $TiO_2$ formula units, $N_{TiO_2}$. We observe that **(i)** $\Delta$SCF and $G_0W_0$ predictions show a significant size dependence, unlike the KS-DFT eigenvalues for which there is hardly any quantum confinement effect. Furthermore, neither the $G_0W_0$ nor $\Delta$SCF quaisparticle energies can be described as a rigid shift from KS-DFT eigenvalues, which means that a simple scissors operator would not allow KS-DFT to reproduce size-dependent effects quantitatively. **(ii)** While the IPs computed with $\Delta$SCF are consistently smaller than those computed with $G_0W_0$ by a roughly constant amount, the EA values computed at these two levels of theory are found to agree fairly well with each other, similar to the trends observed for Si nanocrystals [2] and nanoshells [3]. **(iii)** For the smallest NC with 2 $TiO_2$ units, the offsets of the IP and the EA from the corresponding bulk limits are of similar magnitude, however, as the NC size increases, the EA is found to converge much more slowly to the bulk limit than the IP. We hypothesize that this difference in convergence rates is due to differences in the orbital characters of the HOMO and LUMO of the NCs, which have primarily O $2p$ and Ti $3d$ characters, respectively.

We also employed TDDFT to predict optical properties of NCs up to ~1.5 nm in size. We showed that while TDDFT optical gaps are affected by quantum confinement, they exhibit a weaker size dependence than $GW$ quasiparticle energies, and result in exciton binding energies an order of magnitude larger than that observed in bulk $TiO_2$. Even though the quasiparticle levels of even the largest NC considered in our study have not yet reached the bulk limit and its absorption cross section does not resemble the imaginary part of the bulk dielectric function with its well-defined van Hove singularities, we showed that the "concept" of bulk dielectric function still survives to the (sub)-nanometer size regime. In particular, we showed that the classical Mie-Gans theory, in which the absorption cross section $\sigma_{\rm MG}(\omega)$ can be expressed in terms of the real ($\epsilon_{1i}$) and imaginary ($\epsilon_{2i}$) parts of the $i$th ($i = x, y, z$) component of the dielectric tensor of the bulk material and depolarization factors $G_i$ (related to the dimensions of the NC) as

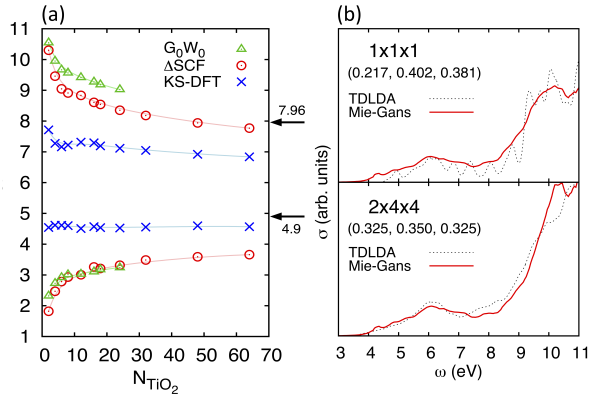


Figure 2: **(a)** Comparison of IPs (above 6 eV) and EAs (below 6 eV) as a function of the number of $TiO_2$ units in the NC, calculated at three levels of theory: $G_0W_0$ (green triangles), $\Delta$SCF (red circles), and KS-DFT (blue crosses). Experimental bulk levels of 7.96 eV and 4.9 eV for IP and EA, respectively, are indicated by arrows at the right. **(b)** TDLDA versus Mie-Gans optical spectra for the $(TiO_2)_2$ (top) and $(TiO_2)_{64}$ (bottom) NCs. The depolarization factors used to compute the Mie-Gans spectra for the NCs are given in each figure.

$$\sigma_{\rm MG}(\omega) \propto \sum_{i=1}^{3} \frac{\omega\epsilon_{2,i}(\omega)}{[1 + G_i[\epsilon_{1,i}(\omega) - 1]]^2 + [G_i\epsilon_{2,i}(\omega)]^2}, \quad (1)$$

can quite accurately reproduce the line shape of TDDFT spectra, as shown in Fig. 2(b) for the case of the smallest (~0.4 nm in size) and largest (~1.5 nm in size) NCs considered in our study. Our results, therefore, suggest that one should exercise caution in modeling the optical properties of macroscale $TiO_2$ particles via the use of small passivated $TiO_2$ NCs and extrapolating the results from these idealized systems to practically bulk-like length scales, as the absorption spectrum of such small NCs will be primarily dominated by Mie surface plasmon resonances.

## 1.2 Excitation Spectra of Aromatic Molecules from Many-Body Perturbation Theory

We performed a detailed analysis of vertical IPs, EAs, and singlet excitation energies on an aromatic molecule test set (benzene, thiophene, 1,2,5-thiadiazole, naphthalene, benzothiazole, and tetrathiafulvalene) computed within the $GW$BSE formalisms [4] (Note that here we use a somewhat unconventional terminology, where IP indicates the binding energy for *any* electron in the neutral molecule, and EA indicates the energy released when adding an electron to *any* unoccupied orbital). We compared $G_0W_0$ results from our real- and transition-space implementation of $GW$ (using RGWBS) with results from a fully plane-wave framework that employed the BerkeleyGW code. Given the myriad differences between the numerical algorithms and convergence techniques between the two codes, the computed $G_0W_0$ energies were found to be in very good agreement with each other, with nearly all energies agreeing to within 0.1 eV for occupied and low-lying unoccupied orbitals.

We then generalized our framework to test variants of the $GW$ approximation that included an LDA-derived vertex function ($\Gamma_{\mathrm{LDA}}$) and quasiparticle-self-consistent (QS) iterations and benchmarked $GW$ energies at four levels of theory: $G_0W_0$@LDA, $G_0W_0\Gamma_{\mathrm{LDA}}$, QS$GW$, and QS$GW\Gamma_{\mathrm{LDA}}$. As shown in Fig. 3(a), we found that $\Gamma_{\mathrm{LDA}}$ leaves energy level spacings nearly the same by shifting up IPs and EAs by a roughly constant $\sim$0.7 eV (orbitals less bound). Quasiparticle self-consistency applied to conventional $GW$ opens up the fundamental gap for all molecules, increasing both hole and quasielectron energies relative to perturbative $GW$. In the combined QS$GW\Gamma_{\mathrm{LDA}}$, the overall change in self-energies is essentially the two independent corrections combined; we did not observe higher-order interactions of quasiparticle self-consistency and $\Gamma_{\mathrm{LDA}}$. Nevertheless, we found the $\Gamma_{\mathrm{LDA}}$ corrections and self-consistency effects to be of

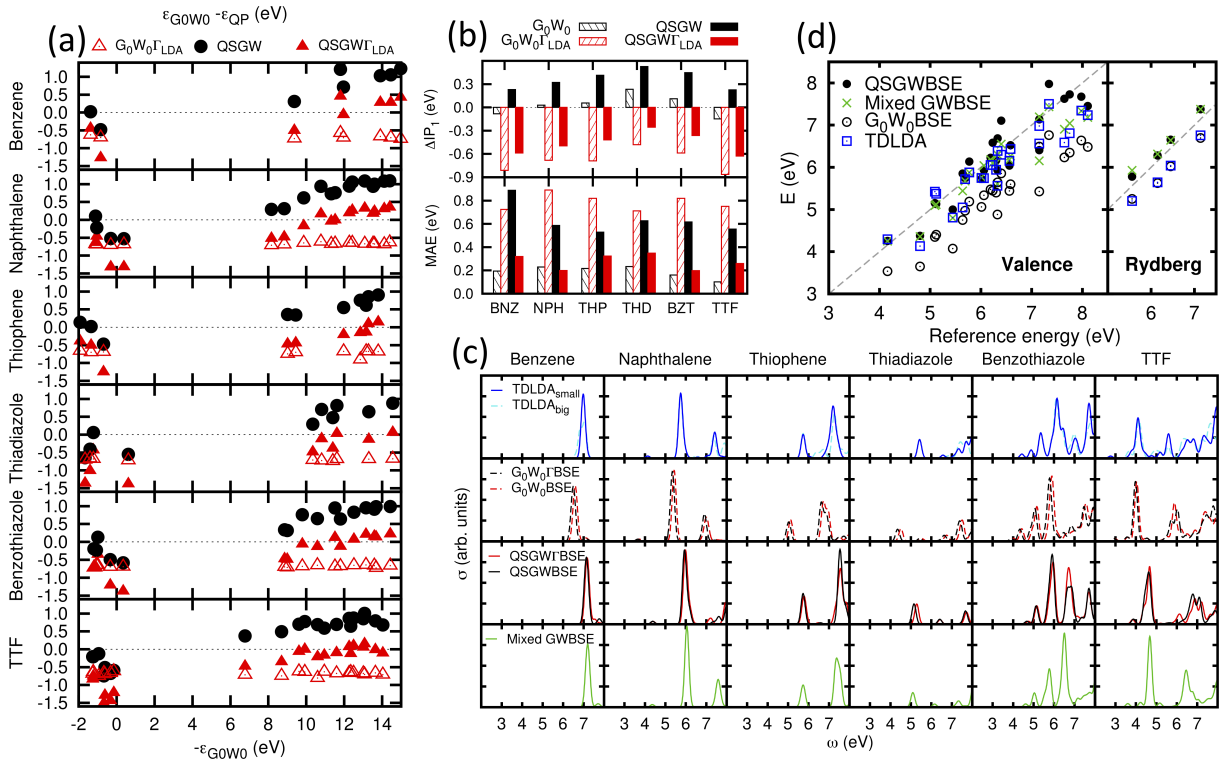


Figure 3: **(a)** Shift of quasiparticles energies from predictions at $G_0W_0$, for $GW$ variants including self-consistency and vertex corrections. **(b)** Error for the first IP (top) and the mean absolute error of orbitals with IPs up to 15 eV (bottom), relative to experiment for each molecule. **(c)** The absorption cross section for each of the molecules, as predicted by various levels of theory. **(d)** The deviation of various first-principles methods relative to best available theoretical values (labeled as reference) for the vertical valence (left) and Rydberg (right) excitation energies.

similar magnitude on our test set. This resulted in a cancellation of effects for IPs, and a compounding of effects for EAs. By comparing to photoelectron spectroscopy measurements for IPs (up to 15 eV) and electron transmission spectroscopy measurements as well as reference CCSD(T) calculations for EAs, we concluded that $G_0W_0$ and QS$GW\Gamma_{\rm LDA}$ are more accurate for IPs [Fig. 3(b)], while $G_0W_0\Gamma_{\rm LDA}$ and QS$GW$ are best for EAs. Altogether, we saw that no single variant of the $GW$ theories was most accurate for both IPs and EAs.

We also computed valence and Rydberg singlet excitations using TDLDA and the BSE formalism with quasiparticle energies computed at the 4 levels of theory mentioned above [Fig. 3(c)]. Since $\Gamma_{\rm LDA}$ leaves relative quasiparticle energies differences unchanged, the addition of this vertex to $GW$BSE calculations (perturbative or self-consistent) typically changes the predicted energies by less than 0.1 eV. The underestimated fundamental gap in perturbative $GW$ results in underestimated excitation energies from perturbative $GW$BSE, while the increased fundamental gap of self-consistent $GW$ is reflected in the corresponding increase in the excitation energies for self-consistent $GW$BSE. We found that for self-consistent $GW$BSE, mean absolute differences from best available previous theoretical values are no larger than 0.33 eV for all molecules, while non-self-consistent $GW$BSE excitation energies have mean errors larger than 1.2 eV, which underscores the importance of self-consistency for obtaining accurate predictions for optical excitations within the $GW$BSE formalism [Fig. 3(d)]. Motivated by the observation that $G_0W_0$ energies have the best agreement with experimental IPs, while $G_0W_0\Gamma_{\rm LDA}$ energies are better for EAs, we also applied BSE to a mixed set of $GW$ quasiparticle energies, where $G_0W_0$ energies are used for occupied orbitals and $G_0W_0\Gamma_{\rm LDA}$ for unoccupied orbitals. This hybrid approach, which we denote as mixed $GW$BSE also yielded optical excitation energies in good agreement with experiment, but at a significantly smaller computational cost due to lack of self-consistency in the input $GW$ energies. Our calculations also confirmed that TDLDA predictions for localized *valence* excitations within *sp*-bonded molecules are in good agreement with higher-level quantum chemistry calculations, However, the LDA functional's incorrect asymptotic behavior results in a deterioration of its accuracy when long-range interactions become important, as in *Rydberg* excitations. The $GW$BSE framework, on the other hand, treats Rydberg and valence excitations on equal footing. We showed that the relatively inaccurate DFT-LDA mean-field starting point is already sufficient to initialize (self-consistent or mixed) $GW$BSE calculations that describe neutral excitations in aromatic molecules with improved accuracy, whether the excitations have valence or Rydberg character.

### 1.3 Excitation Spectra of Group IB and IIB Transition Metal Atoms and Monoxides

We benchmarked the impact of various numerical and theoretical approximations on excitations of Group IB and IIB atoms and monoxide molecules [5], in collaboration with Fabien Bruneval. $GW$ quasiparticle energies were computed for ground state atoms in three valence electron configurations: $d^{10}$ ($Cu^+$, $Ag^+$, $Zn^{2+}$, and $Cd^{2+}$), $d^{10}s^1$ ($Cu^0$, $Ag^0$, $Zn^+$, and $Cd^+$), and $d^{10}s^2$ ($Cu^-$, $Ag^-$, $Zn^0$, and $Cd^0$). For the same species, we also determined low-lying $GW$BSE neutral excitation energies. We compared our pseudopotential $GW$ calculations performed with RGWBS to Gaussian basis-set, all-electron $GW$ calculations performed with MOLGW. For comparison to experimental ionization energies, quasiparticle energies were obtained across six levels of $GW$ theory – $G_0W_0$@LDA, $G_0W_0\Gamma_{\rm LDA}$@LDA, ev$GW$@LDA, ev$GW\Gamma_{\rm LDA}$@LDA, $G_0W_0$@PBE, and ev$GW$@PBE – where ev$GW$ is eigenvalue self-consistent $GW$.

Taking the Zn atom as a test case, we first showed that the complete basis set limit for $GW$ energies can be reached via extrapolation. Improved extrapolations of $d$-state $GW$ energies can be obtained using a static remainder closure relation for the quasiparticle summation [2,6–8], but convergence remains slower than for $s$ and $p$ states, and numerical accuracy is $\sim$0.2 eV [Fig. 4(a)]. We found that energy differences between $G_0W_0$ and ev$GW$ converge more quickly with basis set size than the energy itself. ev$GW$ energies can, therefore, be obtained from a smaller basis set, if the complete basis set limit of the $G_0W_0$ energy is already known. For the BSE, we showed that transitions between $s$ and $p$ orbitals were found to be well converged on finite basis sets, while the numerical accuracy associated with $d$ states was again $\sim$0.2 eV.

We also demonstrated that **(i)** exact exchange in the initial mean-field electronic structure can tune $G_0W_0$ and ev$GW$ energy by $\sim$1 eV, **(ii)** non-hybrid DFT starting points tend to produce lower quasiparticle energies (higher predicted ionization energies), and **(iii)** that no single starting point (with respect to the amount of exact exchange) seems to be optimal for *all* ($s$, $p$, and $d$) orbitals.

In benchmarks comparing perturbative and self-consistent $GW$, accuracies do not improve with eigenvalue self-consistency or the LDA vertex [Fig. 4(b)]. The effect of $\Gamma_{\mathrm{LDA}}$ on the $GW$ calculation is to increase the quasiparticle energies, but in contrast with our work on aromatic molecules, the amount of the shift is not nearly constant, but relates to the localization of the wave function. We showed that $GW$@PBE energies are very similar to those of $GW$@LDA for $s$ and $p$ states, but for $d$ states the $G_0W_0$@PBE is slightly more accurate than any variant of $GW$ that uses a LDA starting point.

For two-particle excitations, we obtained excellent agreement between BSE@$G_0W_0\Gamma_{\mathrm{LDA}}$@LDA eigenvalues and experimental measurements of absorption, as long as *off-diagonal terms are included* in the self-energy contributions [Fig. 4(c)]. The more computationally expensive BSE@ev$GW$@PBE was found to have comparable high accuracy. We observed that a cancellation of errors occurs for the $GW$ quasiparticles, with these two levels of theory producing mean errors $\sim$0.2 eV. These results suggested that inclusion of off-diagonal elements and further development of vertex corrections may be a route to cheaper yet more accurate $GW$BSE computations of optical properties.

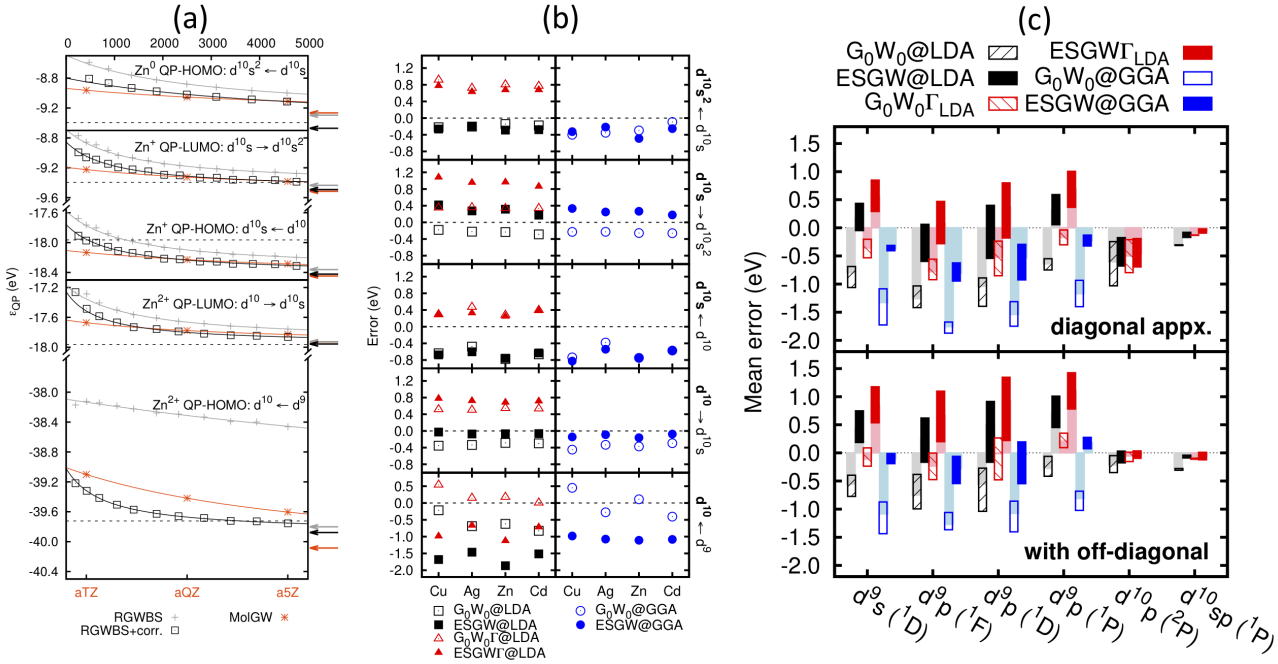


Figure 4: **(a)** $G_0W_0$@PBE energies (eV) for $Zn^0$, $Zn^+$, and $Zn^{2+}$ at varying basis set sizes – aug-cc-pVTZ through aug-cc-pV5Z for MOLGW (bottom axis labels) and up to more than 4000 total states for RGWBS (top axis labels). RGWBS results are shown both with and without a COHSEX correction term added (indicated by "+corr."). Solid lines are extrapolation curves, arrows indicate the extrapolated complete basis set limits, and dashed lines indicate the negative experimentally measured ionization energies. Note that each ionization energy can be compared to the energy of the QP-HOMO for the same species, and the energy of the QP-LUMO for the species with one fewer electron. For example, the top two sets of lines both represent the $d^{10}s \rightarrow d^{10}s^2$ energy, which is the negative of the ionization energy of $Zn^0$; the first set of lines are the QP-HOMO energy of $Zn^0$ ($d^{10}s^2$ valence) at various basis set sizes, and the second set of lines as the QP-LUMO energy of $Zn^+$ ($d^{10}s$ valence). **(b)** Error of $GW$ quasiparticle energies relative to experiment, with reference valence electron configurations given on the right in bold. **(c)** Error of $GW$BSE predictions relative to experimental absorption energies from a $d^{10}$ (first four sets of bars), $d^{10}s$ (fifth set), or $d^{10}s^2$ (sixth set) electron configuration to the configuration listed along the x-axis. Rectangles matching the legend indicate the error range across the Cu, Ag, Zn, and Cd test set, with fainter colored bars providing a guide for the eye.

Our benchmarks of transition metal monoxide anions exhibited differences between $G_0W_0$ and experimental binding energies that are consistent with the benchmarks of the Group IB and IIB single atoms and ions – a few hundred meV, with larger deviations for quasiparticles with more $d$ character. Multiple states can coexist in such energy ranges, and the uncertainty prevented a definitive prediction of excited state energy ordering from the $G_0W_0$ approximation in some cases, such as for $CdO^-$. Therefore, while we were able to limit numerical errors to ∼0.2 eV, scientific questions continue to motivate the search for more advanced techniques in $GW$ theory and computation for transition metal systems.

### 1.4 Photoelectron Spectra of Copper Oxide Cluster Anions

In a collaborative project involving Leeor Kronik and Anna Krylov, we investigated photelectron spectra of copper oxide cluster anions, $CuO^-$, $CuO_2{}^-$, $CuO_3{}^-$, and $Cu_2O^-$. The spectra were computed using various techniques including DFT with PBE, PBE0, and optimally-tuned range separated hybrid (OT-RSH) functionals, many-body perturbation theory within the $G_0W_0$ approximation (with PBE and hybrid functional starting points), and equation-of-motion coupled-cluster methods. We compared results from these first principles methods with each other and experimental data. The results from this study will be submitted for publication to the Journal of Chemical Theory and Computation in late 2017 [9].

The computed photoelectron spectra of the $CuO^-$ cluster show interesting variations across different levels of theory [Fig. 5(a)]. The ground state of $CuO^-$ is a closed shell singlet ($^1\Sigma^+$) that could be roughly described as $3d^{10}2p\sigma^2 2p\pi^4$. The first two photoelectron peaks [$X$ and $Y$ states in Fig. 5(a)] can be interpreted as arising from the removal of $pd\pi^\star$ and $pd\sigma^\star$ electrons from anti-bonding orbitals of significant O $2p$ character leading to the $X^2\Pi$ ground state and $Y^2\Sigma^+$ excited state of CuO, respectively [10, 11]. The broad and noisy band in the 4-6 eV energy range can be interpreted as the detachment of electrons from orbitals of primarily $3d$ character (bonding $pd\sigma$, $pd\pi$ and non-bonding Cu $3d$). A comparison of the computed spectra with experimental data surprisingly shows that PBE provides the best predictions (within 50 meV of experiment) for the positions of the first two peaks. The PBE0 and OT-RSH (with exact exchange fraction $\alpha = 0.2$) predictions are virtually the same, but they significantly underestimate both the IP and the $X-Y$ separation by ∼ 0.5 eV. The OT-RSH predictions with $\alpha = 0$ for the positions of the first two peaks lie between the PBE and other hybrid functional predictions. Our results showed that the $G_0W_0$@PBE results are strikingly poor with both $X$ and $Y$ peaks underestimated by ∼1.4 eV.

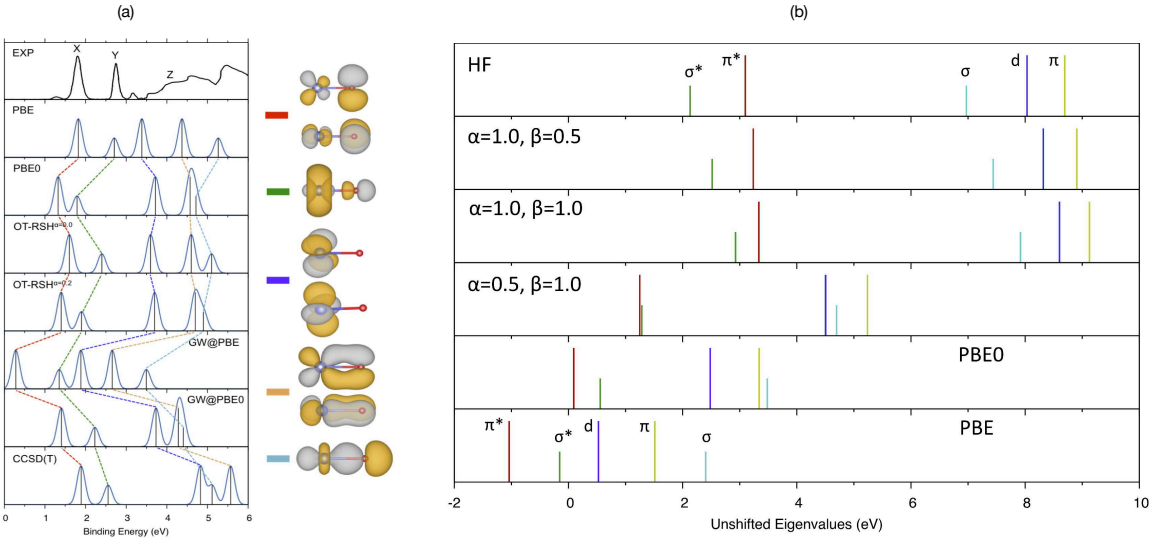


Figure 5: **(a)** Computed binding energies at various levels of theory for $CuO^-$ along with experimental data. Isosurfaces for $pd\pi^\star$, $pd\sigma^\star$, non-bonding Cu $3d$, $pd\pi$, and $pd\sigma$ orbitals at the PBE level are also shown. **(b)** Unshifted eigenvalue spectra computed for differing amounts of Fock exchange and PBE correlation.

PBE0 starting point for $G_0W_0$ calculations significantly improves the quasiparticle energies, but the $X$ and $Y$ levels are still underestimated by $\sim$0.4 eV compared to experiment. Better agreement with experiment can be obtained at the $G_0W_0$@BHLYP level (with 50% exact exchange), where the $X$ and $Y$ peaks are predicted 0.07 and 0.32 eV below the experimental values. Finally, CCSD(T) predictions for the first two peaks (1.89 and 2.56 eV) are within $\sim$0.1 and $\sim$0.2 eV of experimental data. Due to the broad and noisy nature of the Z band, it is not straightforward to make direct comparisons with experiment for states with higher binding energies (BEs). Using the results from CCSD(T) level of theory as a rough guide (which predict three peaks in the 4.5-5.5 eV range, in agreement with experiment [11]), we observe that for these states PBE severely underestimates their BEs, while hybrid functionals do slightly better. Overall taking all five peaks (with BEs less than 6 eV) into account, CCSD(T) performs quite well. PBE predictions are very good for the two most loosely bound states, but they do not perform well for states with higher BEs, while the opposite trend is observed for the case of hybrid functionals.

The increase in the BE of orbitals at the hybrid functional level compared to PBE for orbitals of large Cu 3$d$ character can be understood in terms of mitigation of the self-interaction error by hybrid functionals for localized orbitals via the introduction of a fraction of the Fock exchange [12]. The observation that PBE outperforms PBE0 for the position of the first two $(X, Y)$ peaks is unexpected at first sight, but further analysis allowed us to interpret this finding in terms of the compatibility of exact exchange and correlation: Using an exchange-correlation energy $E_{\rm xc} = \alpha E_{x,\rm HF} + (1-\alpha)E_{x,\rm PBE} + \beta E_{c,\rm PBE}$ where $E_{x,\rm HF}$ is the Hartree-Fock (HF) exchange, and $E_{x,\rm PBE}$ and $E_{c,\rm PBE}$ are semilocal PBE exchange and correlation, respectively, we performed a series of DFT computations varying $\alpha$ and $\beta$ from 0 to 1 [Fig. 5(b)]. Of particular importance is the ordering of the orbitals at the HF level ($\alpha = 1$, $\beta = 0$), where the (non-degenerate) HOMO is incorrectly predicted to be of $\sigma^\star$ character, and the doubly degenerate HOMO-1/HOMO-2 has $\pi^\star$ character. Adding more semilocal correlation to HF decreases the magnitude of the $\pi^\star - \sigma^\star$ separation slightly, but HOMO still has $\sigma^\star$ character even at $\beta = 1$. Upon removing some of the exact exchange, however, the $\pi^\star - \sigma^\star$ ordering gets reversed, and for $\alpha \lesssim 0.5$, HOMO has $\pi^\star$ character, in agreement with experimental data. Therefore, the small $\pi^\star - \sigma^\star$ separation predicted by PBE0 ($\alpha = 0.25$, $\beta = 1$) can be traced to the incorrect description of the ordering at the HF level, with PBE0 having "too much" exact exchange or "not enough" semilocal exchange. Since semilocal exchange is known to mimic static correlation [13–15], we attributed the apparent success of the PBE predictions (for the first two peaks) to a more accurate accounting of static correlation in PBE compared to PBE0.

Similar observations can be made about the predictions of PBE versus hybrid functionals for cluster anions of relatively large O 2$p$ character in low-lying orbitals, such as $CuO_2^-$ and $CuO_3^-$. When the Cu content increases, however, (*e.g.* for $Cu_2O^-$), the overall predictions of PBE compared to hybrid functional predictions significantly worsen. A detailed understanding of correlation effects in systems in which localized $d$ orbitals, less localized $pd$ hybrid orbitals, and even less localized O 2$p$-like orbitals coexist simultaneously is, therefore, a challenging and much needed endeavor, which forms the basis for our future studies.

## 2 Publications Acknowledging This Grant


- Linda Hung, Kopinjol Baishya, and Serdar Öğüt, "A first principles real-space study of electronic and optical excitations in rutile $TiO_2$ nanocrystals", Phys. Rev. B **90**, 165424 (2014).
- Linda Hung, Felipe H. da Jornada, Jamie Souto-Casares, James R. Chelikowsky, Steven G. Louie, and Serdar Öğüt, "Excitation spectra of aromatic molecules within a real-space GW-BSE formalism: Role of self-consistency and vertex corrections", Phys. Rev. B **94**, 085125 (2016).
- Linda Hung, Fabien Bruneval, Kopinjol Baishya, and Serdar Öğüt, "Benchmarking the $GW$ approximation and Bethe-Salpeter equation for group IB and IIB transition-metal atoms and monoxides", J. Chem. Theory Comput. **13**, 2135 (2017).

## References


[1] L. Hung, K. Baishya, and S. Öğüt, "First-principles real-space study of electronic and optical excitations in rutile $TiO_2$ nanocrystals," *Phys. Rev. B*, vol. 90, p. 165424, Oct. 2014.

[2] M. L. Tiago and J. R. Chelikowsky, "Optical excitations in organic molecules, clusters, and defects studied by first-principles Green's function methods," *Phys. Rev. B*, vol. 73, p. 205334, May 2006.

[3] K. Frey, J. C. Idrobo, M. L. Tiago, F. Reboredo, and S. Öğüt, "Quasiparticle gaps and exciton Coulomb energies in Si nanoshells: First-principles calculations," *Phys. Rev. B*, vol. 80, no. 15, p. 153411, 2009.

[4] L. Hung, F. H. da Jornada, J. Souto-Casares, J. R. Chelikowsky, S. G. Louie, and S. Öğüt, "Excitation spectra of aromatic molecules within a real-space $GW$-BSE formalism: Role of self-consistency and vertex corrections," *Phys. Rev. B*, vol. 94, p. 085125, Aug. 2016.

[5] L. Hung, F. Bruneval, K. Baishya, and S. Öğüt, "Benchmarking the $GW$ approximation and Bethe-Salpeter equation for group IB and IIB atoms and monoxides," *J. Chem. Theory Comput.*, vol. 13, p. 2135, Apr. 2017.

[6] W. Kang and M. S. Hybertsen, "Enhanced static approximation to the electron self-energy operator for efficient calculation of quasiparticle energies," *Phys. Rev. B*, vol. 82, p. 195108, Nov. 2010.

[7] J. Deslippe, G. Samsonidze, M. Jain, M. L. Cohen, and S. G. Louie, "Coulomb-hole summations and energies for GW calculations with limited number of empty orbitals: A modified static remainder approach," *Phys. Rev. B*, vol. 87, p. 165124, Apr. 2013.

[8] J. Klimeš, M. Kaltak, and G. Kresse, "Predictive GW calculations using plane waves and pseudopotentials," *Phys. Rev. B*, vol. 90, p. 075125, Aug. 2014.

[9] B. Shi, S. Weissman, N. Orms, A. Krylov, L. Kronik, and S. Öğüt, "Photoelectron spectra of copper oxide clusters from first principles methods," *to be submitted to J. Chem. Theory Comput.*, 2017.

[10] M. L. Polak, M. K. Gilles, J. Ho, and W. C. Lineberger, "Photoelectron spectroscopy of copper oxide $CuO^-$," *J. Phys. Chem.*, vol. 95, pp. 3460–3463, May 1991.

[11] H. Wu, S. R. Desai, and L.-S. Wang, "Chemical bonding between Cu and oxygen copper oxides vs $O_2$ complexes: A study of $CuO_x$ $(x = 0 - 6)$ species by anion photoelectron spectroscopy," *J. Phys. Chem. A*, vol. 101, no. 11, pp. 2103–2111, 1997.

[12] D. A. Egger, S. Weissman, S. Refaely-Abramson, S. Sharifzadeh, M. Dauth, R. Baer, S. Kümmel, J. B. Neaton, E. Zojer, and L. Kronik, "Outer-valence Electron Spectra of Prototypical Aromatic Heterocycles from an Optimally Tuned Range-Separated Hybrid Functional," *J. Chem. Theory Comput.*, vol. 10, pp. 1934–1952, Mar. 2014.

[13] D. K. W. Mok, R. Neumann, and N. C. Handy, "Dynamical and Nondynamical Correlation," *J. Phys. Chem.*, vol. 100, pp. 6225–6230, 1996.

[14] O. V. Gritsenko, P. R. T. Schipper, and E. J. Baerends, "Exchange and Correlation Energy in Density Functional Theory: Comparison of Accurate Density Functional Theory Quantities with Traditional Hartree-Fock Based Ones and Generalized Gradient Approximations for the Molecules $Li_2$, $N_2$, $F_2$," *J. Chem. Phys.*, vol. 107, pp. 5007–5015, Oct. 1997.

[15] S. Kümmel and L. Kronik, "Orbital-Dependent Density Functionals: Theory and Applications," *Rev. Mod. Phys.*, vol. 80, pp. 3–60, 2008.